

# Inelastic x-ray scattering of dense solid oxygen: Evidence for intermolecular bonding

Yue Meng<sup>††</sup>, Peter J. Eng<sup>§</sup>, John S. Tse<sup>¶</sup>, Dawn M. Shaw<sup>¶</sup>, Michael Y. Hu<sup>†</sup>, Jinfu Shu<sup>¶</sup>, Stephen A. Gramsch<sup>¶</sup>, Chichang Kao<sup>††</sup>, Russell J. Hemley<sup>‡¶</sup>, and Ho-kwang Mao<sup>†¶</sup>

<sup>†</sup>High-Pressure Collaborative Access Team, Carnegie Institution of Washington, Argonne National Laboratory, 9700 South Cass Avenue, Argonne, IL 60439; <sup>§</sup>Consortium for Advanced Radiation Source, University of Chicago, 9700 South Cass Avenue, Argonne, IL 60439; <sup>¶</sup>Department of Physics and Engineering Physics, University of Saskatchewan, 116 Science Place, Saskatoon, SK, Canada S7N 5E2; <sup>‡</sup>Geophysical Laboratory, Carnegie Institution of Washington, 5251 Broad Branch Road, Washington, DC 20015; and <sup>††</sup>National Synchrotron Light Source, Brookhaven National Laboratory, P. O. Box 5000, Upton, NY 11973

Contributed by Russell J. Hemley, June 10, 2008 (sent for review February 12, 2008)

The detailing of the intermolecular interactions in dense solid oxygen is essential for an understanding of the rich polymorphism and remarkable properties of this element at high pressure. Synchrotron inelastic x-ray scattering measurements of oxygen K-edge excitations to 38 GPa reveal changes in electronic structure and bonding on compression of the molecular solid. The measurements show that O<sub>2</sub> molecules interact predominantly through the half-filled 1 $\pi_g^*$  orbital <10 GPa. Enhanced intermolecular interactions develop because of increasing overlap of the 1 $\pi_g^*$  orbital in the low-pressure phases, leading to electron delocalization and ultimately intermolecular bonding between O<sub>2</sub> molecules at the transition to the  $\epsilon$ -phase. The  $\epsilon$ -phase, which consists of (O<sub>2</sub>)<sub>4</sub> clusters, displays the bonding characteristics of a closed-shell system. Increasing interactions between (O<sub>2</sub>)<sub>4</sub> clusters develop upon compression of the  $\epsilon$ -phase, and provide a potential mechanism for intercluster bonding in still higher-pressure phases.

high pressure | high-pressure phases of oxygen | molecular interaction | x-ray Raman scattering

Molecular oxygen undergoes a series of phase transitions when compressed at room temperature. Fluid O<sub>2</sub> exists to 5.5 GPa and solidifies upon further compression, forming the rhombohedral  $\beta$ -phase (1) at 5.5 GPa, the orthorhombic  $\delta$ -phase (2) at 9.6 GPa, the monoclinic  $\epsilon$ -phase (3, 4) at 10 GPa, and the modified monoclinic  $\zeta$ -phase (5) at 96 GPa. These transformations are accompanied by marked changes in color, density, and vibrational dynamics (6–9), and by metallization (10), including the appearance of superconductivity at low temperatures (11). These remarkable phenomena in condensed oxygen are consequences of pressure-induced changes in electronic structure and bonding, an area of fundamental importance but previously inaccessible by *in situ* high-pressure studies. Raman and infrared observations of the  $\epsilon$ -phase, specifically the anomaly in the intramolecular vibrational frequencies of O<sub>2</sub> (6, 8) and the appearance of strong infrared absorption (7, 8), have led to suggestions of increased intermolecular interaction, electronic charge transfer, and a paired O<sub>2</sub> model for the  $\epsilon$ -phase. The tendency toward association of O<sub>2</sub> molecules in the  $\epsilon$ -phase was also proposed based on results of early density functional calculations (12). There has, however, been no direct characterization of the molecular interactions in oxygen phases at high pressure.

The recent discovery of (O<sub>2</sub>)<sub>4</sub> molecular clusters in the  $\epsilon$ -phase by x-ray diffraction (3, 4) has revived interest in the nature of the intermolecular interactions in dense fluid and solid oxygen, the evolution of these interactions with pressure, and the origin of the stability of the (O<sub>2</sub>)<sub>4</sub>-based structure of the  $\epsilon$ -phase (13). Using oxygen K-edge inelastic x-ray scattering (IXS) spectroscopy (14), a unique high-pressure probe of local electronic structure and chemical bonding (15–17), we report an experimental characterization of the electronic structure and bonding changes in condensed phases of oxygen up to 38 GPa that

provides direct information on intermolecular interactions on compression. These interactions primarily involve the half-filled 1 $\pi_g^*$  orbital of O<sub>2</sub>; an enhanced intermolecular interaction develops between 1 $\pi_g^*$  orbitals on adjacent molecules, with subsequent orbital delocalization in the low-pressure phases as molecules are brought close together with increasing pressure, leading to intermolecular bonding in the  $\epsilon$ -phase. The chemical bonding in the  $\epsilon$ -phase and its evolution with pressure are discussed.

## Results and Discussion

Representative oxygen K-edge spectra up to 38 GPa at room temperature, where oxygen exists in the dense fluid and solid  $\beta$ -,  $\delta$ -, and  $\epsilon$ -phases, are shown in Fig. 1. Compared with gas-phase O<sub>2</sub> (18) schematically illustrated in Fig. 1, these high-pressure oxygen phases display similar spectral features because of the transitions of 1s core-level electrons to the antibonding 1 $\pi_g^*$  and 3 $\sigma_u^*$  orbitals (hereafter referred to as  $\pi^*$  and  $\sigma^*$  transitions, respectively), which provide a direct indication of their molecular nature. An evident difference, best shown by the K-edge of fluid-O<sub>2</sub> at 3.6 GPa (Fig. 1), is the substantially reduced and broadened second twin peak. This observation is similar to those given in previous reports for solid O<sub>2</sub> films at low temperatures (19–21) and is attributed to a quenching or broadening of the Rydberg states in condensed phases.

Marked changes in  $\pi^*$  and  $\sigma^*$  spectral features with compression are revealed through analysis of the high-pressure IXS spectra as shown in Figs. 2 and 3. These changes clearly define regions of the low-pressure phases and the  $\epsilon$ -phase as a result of differences in the variation of transition energies with pressure. An important result is the distinctly different behavior of the  $\pi^*$  and  $\sigma^*$  transition energies in low-pressure phases (Fig. 2). Compared with that observed in gas-phase O<sub>2</sub>, the  $\sigma^*$  energy displays a noticeable increase of 0.9 eV in the dense fluid phase, followed by a continuous increase with further compression to just below 10 GPa. This behavior is in clear contrast to the  $\pi^*$  energy, which remains constant in this pressure range. At 10 GPa, corresponding to the transition to the  $\epsilon$ -phase (6), there is a discontinuous shift of the  $\pi^*$  transition to a higher energy by  $\sim$ 1.1 eV. For the  $\epsilon$ -phase between 10 and 38 GPa, both  $\pi^*$  and  $\sigma^*$  transition energies increase slightly with pressure. Along with the variation in transition energy, the relative intensity of the  $\pi^*$  feature (Fig. 3), determined from the ratio of the area under the  $\pi^*$  peak to the total signal from 525 eV to 555 eV, shows a considerable decrease with pressure in the low-pressure phases.

Author contributions: Y.M., R.J.H., and H.-k.M. designed research; Y.M., P.J.E., J.S.T., D.M.S., M.Y.H., J.S., C.K., and H.-k.M. performed research; Y.M. analyzed data; and Y.M., P.J.E., J.S.T., S.A.G., and R.J.H. wrote the paper.

The authors declare no conflict of interest.

<sup>†</sup>To whom correspondence may be addressed. E-mail: ymeng@hpcat.aps.anl.gov or r.hemley@gl.ciw.edu.

© 2008 by The National Academy of Sciences of the USA





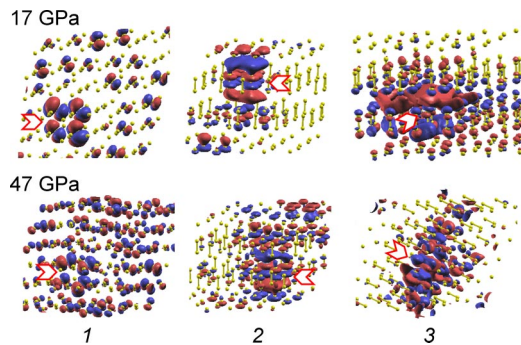


**Fig. 6.** Contour plots of the excited state orbitals, labeled as "1," "2," and "3," corresponding to the three distinct regions of  $\pi^*$ ,  $\sigma^*$ , and the continuum in Fig. 5 at 17 and 47 GPa. The blue and red colored lobes represent the phases of the wave function. The size of the lobes is proportional to the contribution of the atom to the wave function. Smaller lobes localized on an ionized O atom (position marked by arrows) and the concurrent appearance of the lobes in more distant atoms indicate that the final state wave function is more delocalized.

calculated oxygen XAS K-edges of the  $\epsilon$ -phase at selected pressures from 10 to 47 GPa, with the corresponding excited state orbitals plotted in Fig. 6. The spectral features and the qualitative trends of the intensity and energy variations agree reasonably well with the experiment. The calculation also reproduces the appearance of a broad feature at high energies  $\sim 550$  eV as pressure is further increased in the  $\epsilon$ -phase (K-edge at 34 GPa in Fig. 1). The intercluster interaction in the  $\epsilon$ -phase through the  $\pi^*$  orbital is revealed by comparing the K-edges of the solid  $\epsilon$ -phase and an isolated  $(\text{O}_2)_4$  cluster (Fig. 7). The reduced  $\pi^*$  intensity in the  $\epsilon$ -phase as compared with that in the isolated cluster indicates that this orbital in the  $\epsilon$ -phase is more delocalized as a result of interactions between neighboring clusters. With further compression of the  $\epsilon$ -phase, the orbital delocalization increases, as evidenced by the observed continuous decrease in the relative  $\pi^*$  intensity; this conclusion is supported by the theoretical calculations (Figs. 5 and 6). Fig. 6 illustrates that the excited state is delocalized beyond a single  $(\text{O}_2)_4$  cluster at 17 GPa, and the extent of this delocalization is increased at 47 GPa. These results suggest an increase in intercluster interactions with pressure in the  $\epsilon$ -phase. The enhanced role of the  $\sigma^*$  orbital in the high-pressure region of the  $\epsilon$ -phase is further demonstrated by the appearance of the broad feature at  $\sim 550$  eV, assigned to an admixture of the  $\sigma^*$  orbital and the  $\sigma^*$ -like continuum state. The increased intercluster interaction in the  $\epsilon$ -phase is not surprising. Previous x-ray diffraction measurements (3) indicate a marked decrease in intercluster distance; at 47 GPa, the distance between neighboring clusters is comparable with the distance between  $\text{O}_2$  molecules within the cluster at 10 GPa. Such an intercluster interaction provides a possible mechanism for the formation of bonding between adjacent clusters in the  $\zeta$ -phase of oxygen and the onset of metallization at still higher pressure (10).

## Materials and Methods

High-purity oxygen (99.999%) was cryogenically loaded into a sample chamber in an x-ray transparent beryllium gasket compressed in a panoramic diamond anvil cell (DAC). To prevent potential contamination, sample loading was conducted in a controlled environment. Before gas  $\text{O}_2$  was cryogenically liquefied for loading, air was removed from the loading chamber by replicating steps of vacuum pumping and  $\text{O}_2$  gas purging. The purity of the loaded samples was confirmed by optical spectroscopy.

Oxygen K-edge spectra were collected at high pressures by using the inelastic x-ray scattering (IXS) technique at beamlines 16ID-D (HPCAT) and 13ID-C (GSECARS) of the Advanced Photon Source. The two facilities have

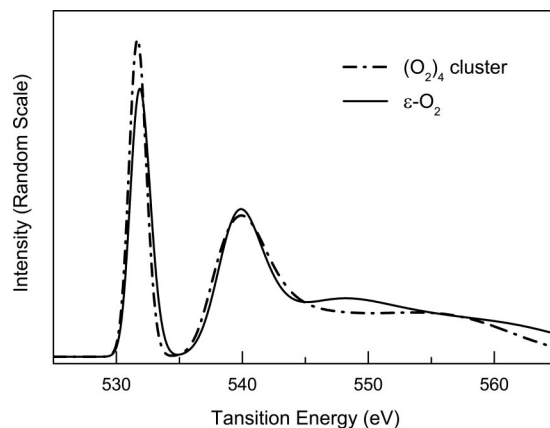


**Fig. 7.** Comparison of calculated K-edge spectra of solid  $\epsilon$ - $\text{O}_2$  and an isolated  $(\text{O}_2)_4$  cluster.

nearly identical IXS setups and use essentially the same major components for the collection of IXS data. By using a pair of meter-long KB mirrors, monochromatic x-rays from an undulator source were focused to a spot of area  $50 \mu\text{m} \times 15 \mu\text{m}$  at the sample position. With the DAC mounted on the rotation center of the IXS spectrometer, we collected oxygen K-edge spectra by scanning the incident beam energy from 525 to 565 eV above the analyzer elastic scattering energy of 9.6865 keV. The scattered x-rays were collected with a six-element Si (660) analyzer positioned at 870 mm from the sample at a  $2\theta$  angle of  $18^\circ$ , and the intensity at the elastic energy reflected by the analyzer crystals was recorded in a near back-scattering (Bragg angle of  $89^\circ$ ) geometry by using an AMPTEK Si detector. The analyzer elastic energy was determined after each experiment setup and the system reliability verified by using the K-edges of standard graphitic phases of carbon and boron nitride. Energies of K-edge spectral features, presented by energy loss (incident photon energy – analyzer elastic energy), are not affected by standard uncertainties in absolute energy calibration. To increase the signal to background ratio, a postsample slit at the  $2\theta$  angle was used to discriminate the signal along the beam direction. Pressures were calibrated by the ruby luminescence method before and after each IXS measurement.

Theoretical O K-edge x-ray absorption spectra (XAS) of the  $\epsilon$ -phase at high pressures were calculated by using the CPMD code (35) with a supercell model consisting of 216 atoms constructed with atomic positions derived from the corresponding fully optimized structure at each pressure by using the PWSCF code ([www.pwscf.org](http://www.pwscf.org)). The calculations used the density function of Perdew *et al.* (36) with the 1s core represented by the Troullier–Martins norm-conserving pseudopotential for the O atom (37) and valence orbitals by a plane wave basis with an energy cutoff of 90 Ry. Only the  $\Gamma$ -point is used for energy sampling. A partially screened half-core hole (38, 39) with half of an electron removed from the 1s core level was used to mimic the ionized O atom. This transition-state model, in principle, takes into account the relaxation effect up to second order in the transition energy. Wave functions of empty orbitals from the transition-state potential, which had been shown to yield reliable oscillator strengths for core-level absorption spectra (40), were used to approximate the final state in the calculation of the K-edge XAS spectra. Oscillator strengths were obtained from the projection of the core wave function to the O 2p projected density of states. This approach has been shown to produce results in reasonable agreement with the experiment (39, 41, 42). Two thousand electronic states, including occupied orbitals, were generated for the calculation, yielding electronic excitations up to 577 eV. Trial calculations using a larger supercell with 512 atoms and 3,000 electronic states show no quantitative change in the calculated XAS profile.

**ACKNOWLEDGMENTS.** We thank S. K. Lee, B. Militzer, and J. B. Neaton for reviewing the manuscript; G. Cody and R. E. Cohen for comments and suggestions; and M. Phillips for coordinating manuscript-related communications. GeoSoilEnviro Consortium for Advanced Radiation Sources (GSECARS) is supported by Department of Energy (DOE)–Basic Energy Sciences (BES)–Geosciences, National Science Foundation (NSF)–Division of Earth Sciences (EAR), and the State of Illinois. The High-Pressure Collaborative Access Team facility is supported by DOE–BES, DOE–Office of Nuclear and National Security Information (Carnegie DOE Alliance Center), NSF, Department of Defense–Tactical Army Command, and the W. M. Keck Foundation.

- Schiferl D, Cromer DT, Mills RL (1981) Structure of O<sub>2</sub> at 5.5 GPa and 299 K. *Acta Crystallogr B* 37:1329–1332.
- Schiferl D, Cromer DT, Schwalbe LA, Mills RL (1983) Structure of 'orange' <sup>18</sup>O<sub>2</sub> at 9.6 GPa and 297 K. *Acta Crystallogr B* 39:153–157.
- Fujihisa H, et al. (2006) O<sub>8</sub> cluster structure of the epsilon phase of solid oxygen. *Phys Rev Lett* 97:085503.
- Lundegaard LF, Weck G, McMahon MI, Desgreniers S, Loubeyre P (2006) Observation of an O<sub>8</sub> molecular lattice in the epsilon phase of solid oxygen. *Nature* 443:201–204.
- Akahama Y, Kawamura H, Hausermann D, Hanfland M, Shimomura O (1995) New high-pressure structural transition of oxygen at 96 GPa associated with metallization in a molecular-solid. *Phys Rev Lett* 74:4690–4693.
- Nicol M, Hirsch KR, Holzapfel WB (1979) Oxygen phase equilibria near 298 K. *Chem Phys Lett* 68:49–52.
- Agnew SF, Swanson BI, Jones LH (1987) Extended interactions in the epsilon-phase of oxygen. *J Chem Phys* 86:5239–5245.
- Gorelli FA, Ulivi L, Santoro M, Bini R (1999) The epsilon phase of solid oxygen: Evidence of an O-4 molecule lattice. *Phys Rev Lett* 83:4093–4096.
- Akahama Y, Kawamura H (2000) High-pressure infrared spectroscopy of solid oxygen. *Phys Rev B* 61:8801–8805.
- Desgreniers S, Vohra YK, Ruoff AL (1990) Optical-response of very high-density solid oxygen to 132 GPa. *J Phys Chem* 94:1117–1122.
- Shimizu K, Suhara K, Ikumo M, Eremets MI, Amaya K (1998) Superconductivity in oxygen. *Nature* 393:767–769.
- Neaton JB, Ashcroft NW (2002) Low-energy linear structures in dense oxygen: Implications for the epsilon phase. *Phys Rev Lett* 88:205503.
- Militzer B, Hemley RJ (2006) Solid oxygen takes shape. *Nature* 443:150–151.
- Hamalainen K, Manninen S (2001) Resonant and non-resonant inelastic x-ray scattering. *J Phys Condens Matter* 13:7539–7555.
- Meng Y, et al. (2004) The formation of sp<sup>3</sup> bonding in compressed BN. *Nat Mater* 3:111–114.
- Mao WL, et al. (2003) Bonding changes in compressed superhard graphite. *Science* 302:425–427.
- Lee SK, et al. (2005) Direct probing of binding changes in B<sub>2</sub>O<sub>3</sub> glasses at high pressure with inelastic x-ray scattering. *Nat Mater* 4:851–854.
- Hitchcock AP, Brion CE (1980) K-shell excitation spectra of CO<sub>2</sub>, N<sub>2</sub>, and O<sub>2</sub>. *J Electron Spectrosc Relat Phenom* 18:1–21.
- Wurth W, et al. (1990) Bonding, structure, and magnetism of physisorbed and chemisorbed O<sub>2</sub> on Pt(111). *Phys Rev Lett* 65:2426–2429.
- Kuiper P, Dunlap BI (1994) The σ\* absorption peak at the oxygen 1s edge of O<sub>2</sub>: Exchange splitting ultrafast dissociation, and atomiclike Auger spectra. *J Chem Phys* 100:4087–4092.
- Ruckman MW, Qiu SL, Chen J, Strongin M (1991) Near-edge study of molecular oxygen and nitrogen clusters on a krypton surface. *Phys Rev B* 43:8603–8605.
- Stohr J et al. (1983) Bonding and bond lengths of chemisorbed molecules from near-edge x-ray-absorption fine-structure studies. *Phys Rev Lett* 51:2414–2417.
- Ruckman MW, et al. (1991) Interpreting the near edges of O<sub>2</sub> and O<sub>2</sub><sup>-</sup> in alkali-metal superoxides. *Phys Rev Lett* 67:2533–2536.
- Outka DA, et al. (1987) Orientation and bond length of molecular-oxygen on Ag(110) and Pt(111): A near-edge x-ray-absorption fine-structure study. *Phys Rev B* 35:4119–4122.
- Stohr J, Sette F, Johnson AL (1984) Near-edge x-ray-absorption fine-structure studies of chemisorbed hydrocarbons—Bond lengths with a ruler. *Phys Rev Lett* 53:1684–1687.
- Bader RFW, Henneker WH, Cade PE (1967) Molecular charge distributions and chemical bonding. *J Chem Phys* 46:3341–3363.
- Pauling L (1960) *The Nature of the Chemical Bond* (Cornell Univ Press, Ithaca, New York).
- Stohr J (1992) *NEXAFS Spectroscopy* (Springer, Berlin).
- Pettersson LGM, Agren H, Vahtras O, Carravetta V (1996) Cluster modeling of core electron photoabsorption of CO adsorbed on Cu(100). *Surf Sci* 365:581–590.
- Ruhl E, Hitchcock AP (1989) Inner-shell excitation of 3d transition-metal carbonyls [Mn<sub>2</sub>(CO)<sub>10</sub>, Mn(CO)<sub>5</sub>Br, and Mn(CO)<sub>5</sub>H] studied by electron energy loss spectroscopy. *J Am Chem Soc* 111:2614–2622.
- Liebman JF, Greenberg A (1988) *Modern Models of Bonding and Delocalization* (VCH, New York).
- Albright TA, Burdett JK, Whangbo M, H (1985) *Orbital Interactions in Chemistry* (Wiley, New York).
- Steudel R, Wong MW (2007) Dark-red O<sub>8</sub> molecules in solid oxygen: rhomboid clusters, not S8-like rings. *Angew Chem Int Ed* 46:1768–1771.
- Tse JS, Yao Y, Klug DD, Desgreniers S (2008) Structure and bonding of the high pressure phases of oxygen. *J Phys Conference Series*, in press.
- CPMD copyright IBM corporation (1990–2004), copyright MPI für Festkörperforschung Stuttgart (1997–2001).
- Perdew JP, Burke K, Ernzerhof M (1996) Generalized gradient approximation made simple. *Phys Rev Lett* 77:3865–3868.
- Troullier N, Martins JL (1991) Efficient pseudo-potentials for plane-wave calculations. *Phys Rev B* 43:1993–2006.
- Slater JC (1974) *Quantum theory of molecules and solids* (McGraw-Hill, New York).
- Triguero L, Pettersson LGM (1998) Calculations of near-edge x-ray-absorption spectra of gas phase and chemisorbed molecules by means of density-functional and transition-potential theory. *Phys Rev B* 58:8097–8110.
- Tse JS, Liu ZF, Bozek JD, Bancroft GM (1989) Multiple-scattering Xα study of the silicon and chlorine core-level photoabsorption spectra of SiCl<sub>4</sub>. *Phys Rev A* 39:1791–1799.
- Cavalleri M, Odelius M, Nordlund D, Nilsson A, Pettersson LGM (2005) Half or full core hole in density functional theory x-ray absorption spectrum calculations of water? *Phys Chem Chem Phys* 7:2854.
- Iannuzzi M, Hutter J (2007) Inner-shell spectroscopy by the Gaussian and augmented plane wave method. *Phys Chem Chem Phys* 9:1599.